Highly transparent and stable flexible electrodes based on MgO/AgNW nanocomposites for transparent heating applications

Abderrahime Sekkat, Dorina Papanastasiou, Maheera Abdul Ghani, Hervé Roussel, Matthieu Weber, Laetitia Rapenne, Carmen Jiménez, David Muñoz-Rojas, Daniel Bellet

ADVANCED MATERIALS TECHNOLOGIES
www.advmattechnol.de

Highly Transparent and Stable Flexible Electrodes Based on MgO/AgNW Nanocomposites for Transparent Heating Applications

Abderrahime Sekkat, Dorina T. Papanastasiou, Maheera Abdul Ghani, Hervé Roussel, Matthieu Weber, Laetitia Rapenne, Carmen Jiménez, David Muñoz-Rojas, and Daniel Bellet**

Transparent electrodes (TE) based on silver nanowire (AgNW) exhibit good physical properties and constitute a promising alternative to transparent conductive oxides due to their low cost, flexibility, and low toxicity. Nevertheless, they suffer from stability issues over harsh conditions, and encapsulation allows to overcome these limitations. Herein, the low-cost, scalable fabrication and study of transparent electrodes based on sprayed AgNW networks coated with MgO thin films deposited by atmospheric pressure spatial atomic layer deposition (AP-SALD) at mild deposition temperature (≤220 °C) is reported. Fabrication of MgO thin films by AP-SALD is reported here for the first time, and their deposition on different substrates is optimized. MgO exhibits a pure phase and conformal growth with a preferential (220) crystalline orientation and a higher growth rate as compared to conventional atomic layer deposition (ALD). Furthermore, thanks to the conformal coating of MgO on AgNW, the obtained nanocomposites exhibit great optical transparency of ≈85% and flexibility while maintaining high stability under thermal and electrical stress. Indeed, this study shows a clear enhancement of the stability of AgNW networks for thin MgO coatings of only a few nanometers thick. Finally, a proof-of-concept transparent heater is fabricated to melt a piece of cheese.

1. Introduction

Transparent Electrodes (TE) are emerging as a leading technology for several optoelectronic applications, such as solar cells, low-emissivity coatings, and organic light-emitting diodes,[1–4] due to their high optical transparency (>90%) and electrical conductivity (<10 Ω sq^{-1})[5] as they are also used as transparent heaters (TH). Initially developed for anti-fog airplane windshields, TH have gained increasing popularity in recent years for various applications, including smart windows, lab-on-chips devices, and thermotherapy.[6] As they satisfy the majority of requirements, in terms of functional characteristics, transparent conducting oxides (FTO, ITO, and AZO) have been the most widely used candidates to date.[7] Nevertheless, they demonstrate several drawbacks, such as material scarcity (specifically for indium), fabrication

A. Sekkat, D. T. Papanastasiou, M. A. Ghani, H. Roussel, M. Weber, L. Rapenne, C. Jiménez, D. Muñoz-Rojas, D. Bellet
Univ. Grenoble Alpes
CNRS
Grenoble INP
LMGP
Grenoble 38000, France
E-mail: david.munoz-rojas@grenoble-inp.fr; daniel.bellet@grenoble-inp.fr

A. Sekkat
Laboratoire de Génie Chimique
Université de Toulouse, CNRS, INPT
Toulouse 31432, France

D. T. Papanastasiou
The University of Tokyo, CNRS-IIS IRL 2820
LIMMS
153-8505 Tokyo, Japan

The ORCID identification number(s) for the author(s) of this article can be found under https://doi.org/10.1002/admt.202301143

DOI: 10.1002/admt.202301143

cost, plasmonic absorption (resulting in low transmittance in the IR range of the spectrum), and brittleness, which drive the community to explore flexible, low-cost, and abundant alternatives for next-generation TH applications.[8]

In this sense, AgNW networks represent a promising TE candidate as they exhibit excellent mechanical properties with a high figure of merit (FoM, optical transparency versus electrical conductivity) comparable to metal oxides.[5,9] Their potential was initially demonstrated in photochromic displays.[10] Despite these properties, AgNW-based TE exhibit a lack of stability and aging issues under ambient and harsh conditions leading to silver oxidation or sulfidation. In addition, thermal and/or electrical stresses induce morphological evolution of the nanowires ultimately leading to loss of AgNW network percolation nature.[5,11] Stability enhancement by encapsulation has been the subject of several reports using oxide and polymer-based thin films.[8,9] In particular, oxides such as Al_2O_3,[12] ZnO,[13] AZO,[14] and TiO_2,[15] have proven to be very efficient. While the enhanced stability comes at the expense of a slight loss of transparency, obtained FoM are acceptable for many applications. In addition, the use of oxide bilayers, namely ZnO/Al_2O_3,[16] can improve the transparency. Finally, apart from preventing their degradation, this strategy allows the combination of complementary properties that are beneficial for specific applications, such as the case of memristive devices based on AgNW/TiO_2[17] or transparent biochip heaters based on AgNW/ZnO.[18] Other materials based on oxynitrides and reduced graphene oxide also show an overall improvement of the operational resilience of the AgNWs.[19,20]

Magnesium oxide (MgO) is a material with advantageous and distinctive characteristics, such as high physical and chemical stability, high transparency and significant insulation properties.[21] This opens up a wide variety of possibilities for its use since it has a high optical bandgap (4-6 eV) allowing for a higher transparency.[22–24] MgO has been developed as a thin film using different processes such as spray,[25] sol-gel,[26] sputtering,[27] and chemical vapor deposition[28] techniques. In addition, ALD has been widely used for the growth of MgO thin films since the 1990s due to its precise growth control of conformal and uniform thin films as a result of the self-limiting, surface, and sequential reactions.[29–37] A promising alternative to ALD, known as AP-SALD, involves separating the precursor in space rather than time with continuous injection of the precursor.[38] Such approach results in higher deposition rates than conventional ALD,[39–41] and has been explored for the growth of high-quality materials for many optoelectronic applications at atmospheric pressure and low deposition temperatures.[42–46] However, to the best of our knowledge, there are no studies so far reporting the AP-SALD deposition of MgO.

In this work, we report the deposition of high-quality, pure and uniform MgO thin films on glass and polymer substrates for the first time by AP-SALD. A higher growth rate was demonstrated compared to what has been reported by ALD processes. The material and structural properties of the film are presented. Encapsulation of AgNW by an optimized MgO thin film has been confirmed and presents a significant stability enhancement against thermal, electrical and mechanical stresses using only a few nanometers thick MgO films. This proves the potential of using such thin films as successful encapsulation for AgNW, especially if the goal is to retain high optical transparency and enhance the stability. Finally, we demonstrate a proof-of-concept of a TH for the fast melting of solid cheese, showing its potential use for applications in which robust transparent heaters are needed.

2. Results and Discussion

The bare AgNW networks were deposited on glass and flexible substrates using spray-coating technique, as detailed in the experimental section. **Figure 1**a illustrates the deposition process of AgNW and the growth of MgO by AP-SALD on top of the network. As reported in previous studies, bare networks undergo spheroidization of the nanowires after thermal annealing,[11] while MgO/AgNWs, in our case, show high stability and flexibility. The SEM image on the left shows bare AgNWs that have been spheroidized induced by a thermal ramp up to 400 °C with a rate of 5 °C min^{-1}, resulting in a complete degradation of the network. The SEM image on the right of Figure 1a shows a AgNWs network coated with MgO thin film and submitted to a similar thermal stress as the bare sample on the left of the figure (400 °C), showing no degradation. The deposition of MgO was carried out at different deposition temperatures (from 200 to 260 °C) on a glass substrate. The XRD spectra, shown in Figure S1a (Supporting Information), reveal that the increase in the thermal budget has no impact on the crystallinity of the MgO thin film, showing in all cases a preferential orientation along <220>. Given that no substantial change in crystallinity is observed with deposition temperature, 220 °C was kept for the remaining of the study. XRD measurements of films having different thicknesses are shown in Figure 1b, and show that the preferential orientation along the <220> direction does not change with thickness. XPS measurement were performed on the Mg 2p for a MgO sample deposited at 220 °C, as presented in Figure S2 (Supporting Information), where the peak at 50.7 eV corresponds to Mg in the +2-oxidation state. In addition, the XPS measurement confirms that carbon can only be seen as traces in the film, depicting the purity of the layer prepared by SALD. The O 1s spectra decomposition indicates that the primary contribution arises from the metallic O—Mg bond, supplemented by the presence of OH and O—C contributions. The optical properties of the different films were evaluated and revealed that they are not impacted by film thickness, with the bandgap varying only slightly from 4.44 to 4.41 eV as thickness increased (Figure 1c). The total transmittance and reflectance of the MgO thin film with different thicknesses, used for the Tauc plot calculations, are presented in Figure S3 (Supporting Information), showing the high film transparency across the different temperatures. The haze factor values of the TH (measured at 550 nm) are reported in Table S1 (Supporting Information). For thin MgO coating (thickness between 10 and 50 nm) the haze factor is not influenced by the coating and is ≈6.2%. Such value stems for the AgNW dimensions and areal mass density of the associated AgNW network, as discussed elsewhere.[3] However, for MgO coating thicker than 50 nm, there is a clear increase of the haze factor: 8.95 and 13.8%, respectively, for the 100 and 200 nm thick MgO layer thickness. Such increase of the haze factor for thicker MgO coating stem from the presence of surface morphologies (such as tips, sharp edges, and corners) that can act as efficient light scattering centers. Therefore, one can play not only with the AgNW

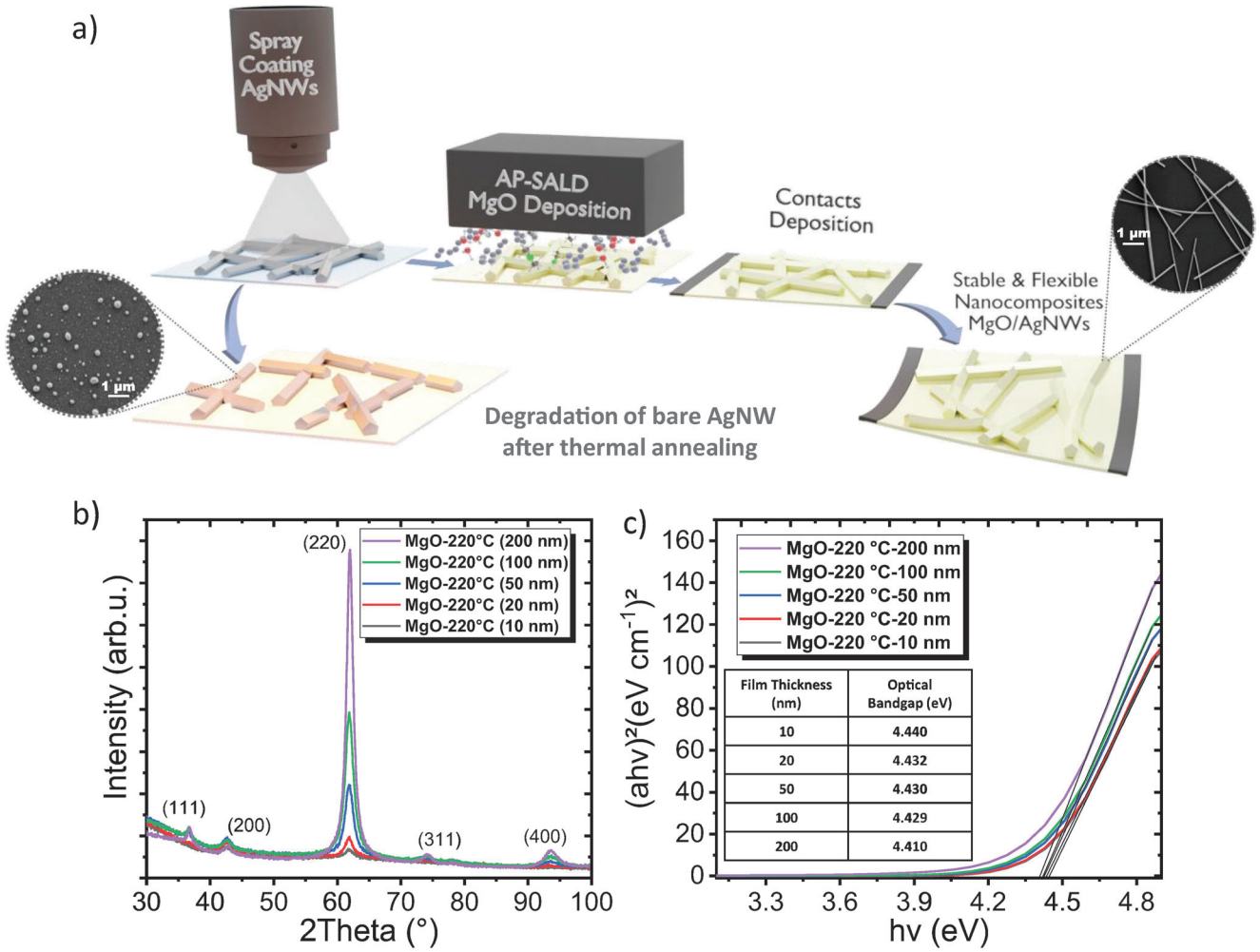

Film Thickness (nm)	Optical Bandgap (eV)
10	4.440
20	4.432
50	4.430
100	4.429
200	4.410

Figure 1. a) Schematic illustration presenting the fabrication steps of stable and flexible MgO/AgNW nanocomposites, by spray coating for AgNW and AP-SALD for MgO film, respectively. As shown in the SEM images in circles, bare AgNW networks degrade after thermal annealing up to 400 °C with 5 °C min^{-1} while the encapsulation with MgO protects them efficiently. b) XRD pattern and c) optical bandgaps, of MgO thin films with different thicknesses (from 10 to 200 nm) deposited at 220 °C by AP-SALD on glass substrate.

dimensions and network areal mass density to tune the haze factor, but also with the MgO coating thickness. This is of key importance for device integration since the required haze factor depends on the targeted applications. Ellipsometry and XRR measurements (see Figure S4, Supporting Information) reveal a large difference in film thickness from 10 to 200 nm with a mean growth per cycle (GPC) of 0.25 ± 0.02 nm per cycle, as compared to a GPC of 0.14 nm per cycle reported for conventional ALD.[32]

Figure 2a shows a TEM image of a thin MgO nanofilm, with a thickness of 2–3 nm, that was grown on top of an AgNW network. There is a slight variation in thickness along the nanowire, possibly attributable to the electron beam degradation caused by the small film thickness and/or due to the observed region being located at the tip of the nanowire. This appears to be more homogeneous for thicker layers over 65 nm, which demonstrates a quite conformal growth overall in the AgNW (Figure 2b). Furthermore, SEM imaging of pristine samples before thermal stress (Figure 2c), confirms that thin MgO layers on top of AgNW have a smooth, conformal morphology, and the deposition is free of pinholes. The thicker layer covers with the same conformal way the nanowires with a much rougher surface. This is confirmed by another SEM image with higher magnification of the 65–70 nm thick film covering the AgNWs as presented in Figure S5 (Supporting Information). Both samples depict a low standard deviation of 0.19 of thickness variation for 2–3 nm thick samples, while 0.29 for 65–70 nm thick coating.

The SEM images in Figure 2c show that subjecting the samples to a thermal annealing, from room temperature (RT) to 400 °C, deteriorate significantly the bare AgNW samples as the nanowires tend to form small spheres caused by the high thermal budget[47] (see methods from more details). The driving force of such degradation is the reduction of the surface energy (i.e., Plateau-Rayleigh instability). Interestingly, the deposition of a thin MgO film with only 2–3 nm prevents the network degradation. In the case of thicker MgO encapsulating films, as observed

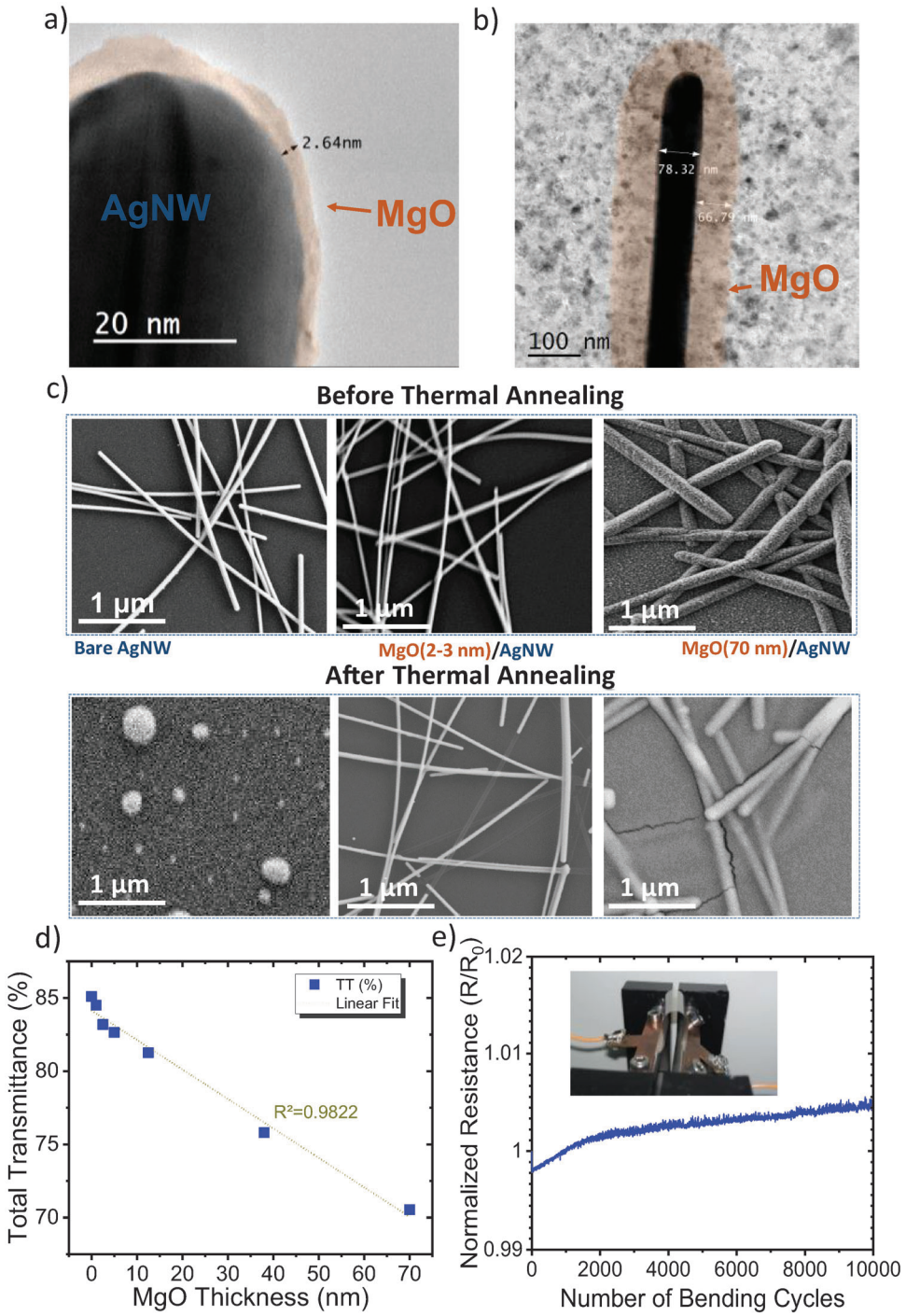

Figure 2. TEM images of MgO thin films deposited on top of AgNW network having a thickness of a) 2–3 nm and b) 65–70 nm. c) SEM images of bare and MgO-coated AgNW networks on glass before (top) and after (bottom) thermal stress. d) The dependence of MgO/AgNW nanocomposite optical total transmittance measured at 550 nm wavelength versus the MgO film thickness. e) The evolution of normalized electrical resistance of MgO/AgNW nanocomposite during 10000 bending cycles with 5 mm radius. The inset picture shows the sample fixed on the bending set-up.

in Figure 2c, the thicker films tend to keep the network steady, even if there are some cracks that exist over the grown thin film.

Following that, we investigated the properties of MgO/AgNW nanocomposites with AgNW networks deposited with the same network density and coated with varied MgO film thicknesses from 1 to 70 nm at 220 °C. Pictures of the actual samples are shown in Figure S6 (Supporting Information). Their optical properties and their performance under thermal, electrical and mechanical stress are discussed in the following sections. The optical transmittance is the key in several devices and the

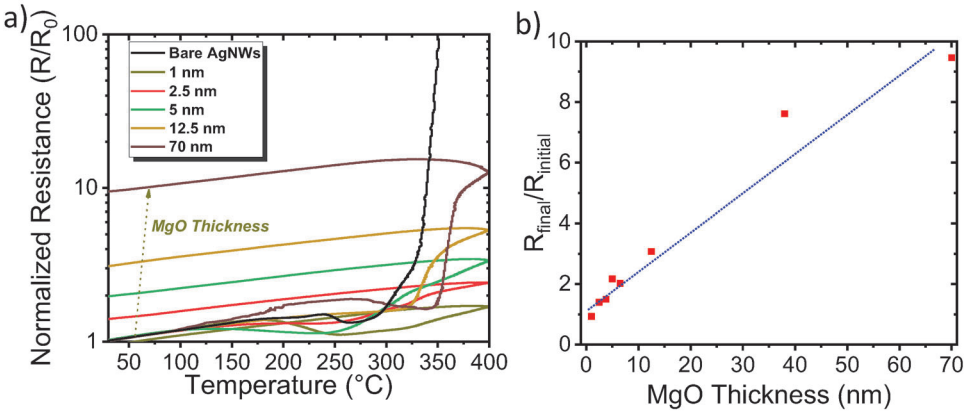

Figure 3. a) Variation of the normalized electrical resistance (R/R_0) of bare and MgO/AgNW networks during a thermal annealing in open-air from room temperature to 400 °C with a ramp of 5 °C min^{-1}. The arrow indicates the increase of MgO thickness b) Ratio between final and initial resistance of MgO/AgNW networks after the thermal annealing at 400 °C.

optimum is to coat the AgNW network with a thin film that manages to increase the stability over harsh conditions without reducing too much its transparency. The measurements performed on coated samples have demonstrated that the total transmittance at 550 nm decreases quite slightly for samples coated with 1 to 5 nm thick MgO, compared to bare AgNW networks, as this value is reducing from 85% to 82% (Figure 2d). This value reduces gradually with the MgO thickness increase until it reaches 70% for 70 nm thick films. A fit of this variation reveals an R^2 value of 98% which demonstrates a linear dependence with respect to the film thickness and allows the extraction of the optical absorption coefficient following this formula:

$$\alpha = -\frac{\ln(1-A)}{t} \quad (1)$$

where α is the optical absorption coefficient of the MgO thin film on a glass substrate and t represents the MgO thickness. As shown in Table S2 (Supporting Information), the absorption coefficient tends to decrease from 1.10^4 to 2.10^3 cm^{-1} due to the increase of MgO thickness and the contribution of its optical properties. Several studies have reported the optical absorption coefficient of MgO, with values ranging from 10^2 to 10^3 cm^{-1},[48,49] which is consistent with the value obtained in this study. The agreement is only valid for one order of magnitude since in the present case the absorption coefficient is larger compared with literature values. This could be explained by the fact that literature mainly reports on film processed by ALD process whereas SALD film may have different structure and morphology (which can exacerbate different light scattering and absorption phenomena). Therefore this is in alignment with the obtained results as the contribution of the MgO thin films tend to intervene from film thickness above several nanometers.

A flexible sample with 1.3 nm thick MgO film covering the AgNWs was used to test its mechanical stability (Figure 2e). The sample shows a very stable behavior without significant increase in the electrical resistance, even after 10000 bending cycles of 5 mm radius. This shows the high flexibility of the fabricated nanocomposite.

The main goal of coating AgNW by MgO is to enhance AgNW network stability. As presented in **Figure 3**a, thermal annealing is performed on bare and coated samples with different thicknesses in order to assess the MgO coating influence of AgNW network stability. The bare sample degrades quite rapidly after the sintering step at ≈275 °C,[11] with a significant and irreversible increase of its electrical resistance. This is associated to the morphological instability shown in Figure 1c for bare AgNWs which eventually leads to the loss of the percolative nature of the bare AgNW network. The sample with 70 nm thick MgO layer seems to prevent the rapid degradation of the network by delaying its increase in normalized resistance up to 350 °C and with an order of magnitude from the starting resistance. Remarkably, this degradation is attenuated when considering thinner MgO layers, with thickness between 1 and 5 nm. Such coated AgNW networks preserve the AgNW morphology after being annealed at 400 °C with a thermal ramp of 5 °C min^{-1} with a negligible change in the normalized resistance, as indicated by the ratio $R_{Final}/R_{Initial}$ shown in Figure 3b. This is quite promising since thinner films result in higher optical transparency as shown in Figure 2d.

Let now consider the origin of the observation that thick MgO layers are not favorable to efficient stability, as one would expect the inverse mechanism (i.e., a better protection from thicker layers, as it has been shown previously for instance for AgNW-ZnO based transparent electrodes[13]). The MgO coating is deposited on both glass substrate and AgNW network, both heated at 220 °C. Due to the difference in thermal expansion coefficient between the glass substrate (α_{glass}) and the MgO thin film (α_{MgO}), one expects that the latter will experience stress after cooling from 220 °C to room temperature. The associated strain, ε, is directly proportional to the thermal expansion coefficient difference ($\Delta\alpha = \alpha_{MgO} - \alpha_{glass}$) and the temperature difference ($\Delta T = 220$ °C):

$$\varepsilon = \Delta\alpha \times \Delta T \quad (2)$$

Such strain is associated to a stress, σ, given in first approximation by:

$$\sigma = \Delta\alpha \times \Delta T \times E \quad (3)$$

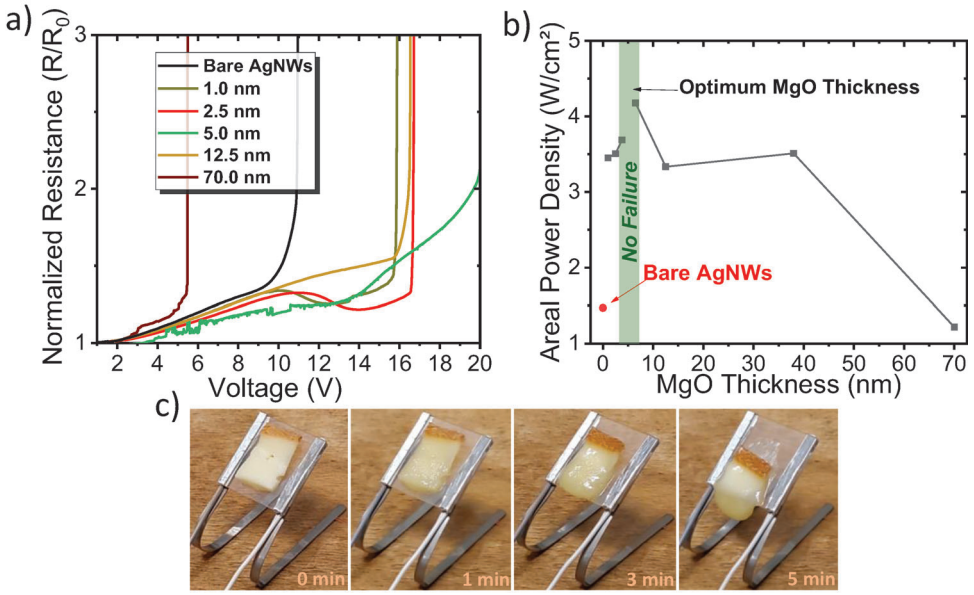

Figure 4. a) In situ variation of the normalized electrical resistance for bare and MgO-coated AgNW networks during a voltage ramp of 0.5 V min^{-1} associated with different MgO layer thicknesses. b) The observed maximum areal power density versus MgO layer thickness. c) The transparent heater demonstration with 12.5 nm thin MgO-coated AgNW nanocomposite for melting local French cheese (Raclette).

where E is the Young modulus of the MgO layer. When the induced stress is larger than the rupture stress, $\sigma_{Rupture}$, then the MgO film can exhibit mechanical degradation, that is, crack formation. α_{MgO} was estimated to $10.4 \times 10^{-6} \times K^{-1}$,[50] α_{glass} close to 7×10^{-6} K^{-1}, while E is close to 300 GPa.[51] Therefore, the stress associated to cooling down the thin MgO layer corresponds roughly to 180 MPa. This value has to be compared with MgO rupture stress, $\sigma_{Rupture}$, which was estimated between 100 and 200 MPa.[51] This means that this simple estimation appears to be in good agreement with the experimental observations, and the difference between thermal expansion of glass and MgO thin film can explain the presence of cracks within MgO layer, as revealed by the SEM imaging (see Figure 2c). However, this approach should be considered with care, since the real physicochemical processes might be more complicated than this model approximation.

The presence of AgNWs on the substrate can create many structural defects in the MgO layer. Moreover, if the latter is very thin, that is, a few nanometers as elaborated in the present work, it can exhibit properties rather different compared with bulk MgO. In any case, this calculation clearly indicates that the stress level within the MgO layer can explain the existence of the observed cracks. One can expect that very thin MgO layer can accommodate such stress, but not in the case of a thicker layer; which explains why a thin MgO layer appears as a more efficient coating compared to a thick MgO layer.

Such stability enhancement was also confirmed for the electrical stress test performed on the bare and coated samples, as presented in **Figure 4**a. The thinner layers (1–12.5 nm) degraded at a higher voltage (≈17 V), which is quite high compared to bare AgNW networks that tend to degrade at 10 V. The thicker MgO case (70 nm) degraded at a low voltage value, which means that it is not efficient for the stable encapsulation of AgNW networks. Furthermore, the enhanced performance is also represented in Figure 4b, where the thin MgO films (1–12.5 nm) show a higher areal power density at electrode failure of 3.5–4 W cm^{-2} compared to the bare AgNW and the thick MgO coated AgNW networks (70 nm), which show a value around 1.5 W cm^{-2}. Infrared images are presented in Figure S7 (Supporting Information), presenting the maximum surface temperature evolution of the samples with respect to different voltage values during the 0.5 V min^{-1} applied electrical ramp. The maximum temperature reached with bare samples is much lower (218 °C) than with thinner coatings, reaching 342 °C, and with thicker coatings, ≈290 °C. Interestingly, the 5 nm thick coated films show no failure of the nanocomposites, even at voltage values that reach 20 V, proving the high encapsulation efficiency of the MgO thinner films against the electrical stress.

Finally, a transparent heater was fabricated by coating 12.5 nm thick MgO in order to melt raclette cheese on the surface of the glass substrate through joule heating (Figure 4c). The cheese sample (initial resistance of 14 Ω) was heated by an applied constant voltage of 4 V, reaching 75 °C and a final resistance of 15.5 Ω. As shown in Figure 4c, we can clearly notice that the cheese starts to melt after 1–3 min and is completely melted after 5 min. The samples are quite robust due to the efficient protection of the AgNW networks provided by the MgO coating, which provides a calculated areal power density of 0.2 W cm^{-2} (2065 W m^{-2}) at 75 °C. This result aligns well with the dependence of areal power density on the stabilized temperatures when compared to previously reported data for various TH technologies.[5] This proof-of-concept is a simple demonstration of the viability of such nanocomposite to be used in transparent heater applications.

3. Conclusion

In summary, AgNW networks have been coated with different MgO thicknesses and showed efficient and stable electrical

performance during thermal and electrical stress. For this purpose, we have developed for the first time MgO thin films by AP-SALD deposited at low temperature (≤220 °C) and characterized their optical and structural properties. We have demonstrated that the films are crystalline along the (220) plane, pure, and free of impurities, as evidenced by the characteristic peak of the MgO phase from XRD, XPS, and XRR measurements. Further, transparent and conductive electrodes have been fabricated by coating silver nanowires with MgO thin films. Remarkably, the electrodes protected by thin MgO films were the most stable (until 400 °C under thermal stress and no failure under electrical stress), since the thicker films can form defects in the lattice (such as cracks easily observed by SEM), which accelerate the degradation. The high bandgap of MgO (4.4 eV) along with the thin coatings that stabilized the AgNW networks, led to electrodes having a high optical transparency of ≈85% and thus a high figure of merit. Finally, a proof-of-concept for melting robust cheese has been elaborated to demonstrate the potential use of the MgO/AgNW nanocomposite as a transparent heater. The composite electrodes presented here can be easily fabricated by low-cost/low-temperature approaches. This, in combination with the obtained superior performances, made these technologies very appealing for integration in mass-produced devices, such as transparent heaters, solar cells, touch screens or low-emissivity coatings.

4. Experimental Section

AgNWs Deposition: 0.1 g L^{-1} suspensions in methanol of AgNWs with an average diameter of 79 ± 10 nm and an average length of 7 ± 3 µm[52] were used (kindly provided by Dr. J.-P. Simonato's group, CEA-LITEN). For the spraying coating of the AgNW solution, a homemade set-up was used, composed of a spray gun, robotic arms that can move along two perpendicular directions and a heating plate.[52] Corning glass substrates (1.1 mm-thick) were cut in size of 2.5 × 2.5 cm^2, cleaned in isopropanol ultrasonic bath, rinsed with distilled water and dried with N_2. The glass or flexible substrates (Neopulim, Mitsubishi-0.1 mm-thick) were placed on top of an aluminum plate that was heated up to 110 °C in order to allow immediate evaporation of solution solvent. The distance between the airbrush nozzle and the substrates was fixed at 7 cm. The flow of solution is regulated by the air pump connected to the airbrush and the pressure used is 1.4 bar. The flow rate of one droplet every about 4 s was adjusted using the needle's position inside the airbrush.

AP-SALD Deposition: The deposition of the MgO thin films was performed using an AP-SALD open-air and scalable approach based on a manifold head, as reported previously.[40] The latter contains one metal precursor outlet, separated from the co-reactant outlets by inert gas barriers alternatively located in between the reactive gas flows to prevent them from mixing.[40] The precursor, bis(ethylcyclopentadienyl)magnesium was heated at 85 °C and the transport line between the bubbler and the manifold injection head was heated at 90 °C to avoid any condensation of the precursor in the lines. A flow of 60 sccm of nitrogen was used for the Mg precursor, which was diluted in extra nitrogen flow (60 sccm) before being sent to the injection head. Finally, the nitrogen barrier flow was adjusted to obtain a flow of 120 sccm per outlet. A flow of 120 sccm of water was diluted with an additional 120 sccm of nitrogen flow. The precursor and co-reactants were injected continuously from the manifold head onto the substrate that oscillated at a scanning speed of 10 cm s^{-1}. The gap between the head and the substrates was maintained at a distance of 150 µm in all cases. Films were deposited on borosilicate glass substrates with a surface area of 3 × 5 cm^2. The substrates were previously cleaned with isopropanol in an ultrasonic bath for 5 min and then dried with N_2.

Characterization Techniques: Film thickness was estimated by ellipsometry (using a compact Film Sense FS-1 ellipsometer). The surface morphology and thickness of the thin films and MgO/AgNW nanocomposites were evaluated by scanning electron microscopy (SEM-FEG, GeminiSEM 300) and with transmission electron microscopy (TEM) (JEOL JEM 2010 LaB6 microscope operating at 200 kV with a 0.19 nm point-to-point resolution). AgNWs/MgO nanocomposites were directly deposited on carbon-coated copper grids for TEM observations. X-ray Diffraction patterns were obtained with a Bruker D8 Advance diffractometer in the Bragg-Brentano (θ–2θ) configuration, with Cu Kα1 radiation (0.15406 nm). The optical properties of the films were evaluated with a Perkin Elmer lambda950 UV-Vis-NIR spectrophotometer within the wavelength range of 250–2500 nm. The optical bandgaps of the different films were extracted from the transmittance and reflectance spectra using the Tauc plot method. XPS measurements were performed using a ThermoScientific K-Alpha spectrometer with an Al Kα (1486.6 eV) X-ray source. The samples were pretreated with an Ar-ablation process at 2 keV for 60 s.

Device Fabrication and Testing: The transparent heater (TH) based on MgO/AgNWs nanocomposites was covered on the edges with a silver paste (L-200N, CDS Electronique) that was dried for 1 h in the ambient. Copper cables were connected directly on top of the silver paste contacts with a silver tape to maintain them steady all over the measurements. A Keithley2400 sourcemeter was connected to the TH providing a constant voltage of 4 V for several minutes.

Supporting Information

Supporting Information is available from the Wiley Online Library or from the author.

Acknowledgements

A.S. and D.T.P. contributed equally to this work. This work was partially supported by the CDP Eco-SESA, receiving funds from the French National Research Agency in the framework of the "Investissements d'avenir" program (ANR-15-IDEX-02)" and by the M-Era-Net project INSTEAD. The authors acknowledge the Agence Nationale de la Recherche (ANR, France) via the projects DESPATCH (ANR-16- CE05-0021), ALD4MEM (ANR-20-CE09-0008) and Institut Carnot Energies du futur. The authors would like to warmly thank Jean-Pierre Simonato for fruitful discussions. This research has benefited from the characterization equipment of the Grenoble INP–CMTC platform supported by the Centre of Excellence of Multifunctional Architectured Materials "CEMAM" noANR-10-LABX-44-01 funded by the "Investments for the Future" Program. This work benefited from the facilities and expertise of the OPE)N(RA characterization platform of the FMNT (FR 2542) supported by CNRS, Grenoble INP and UGA.

Conflict of Interest

The authors declare no conflict of interest.

Data Availability Statement

The data that support the findings of this study are available from the corresponding author upon reasonable request.

Keywords

AP-SALD, flexible devices, silver nanowire networks, transparent electrodes, MgO

Received: July 11, 2023
Revised: September 20, 2023
Published online: November 1, 2023

[1] Y. Zhang, S. Ng, X. Lu, Z. Zheng, *Chem. Rev.* **2019**, *10*, 1021.
[2] J. Yun, *Adv. Funct. Mater.* **2017**, *27*, 1606641.
[3] T. Sannicolo, M. Lagrange, A. Cabos, C. Celle, J. P. Simonato, D. Bellet, *Small* **2016**, *12*, 6052.
[4] S. Hanauer, C. Celle, C. Crivello, H. Szambolics, D. Muñoz-Rojas, D. Bellet, J.-P. Simonato, *ACS Appl. Mater. Interfaces* **2021**, *13*, 21971.
[5] D. T. Papanastasiou, A. Schultheiss, D. Muñoz-Rojas, C. Celle, A. Carella, J. P. Simonato, D. Bellet, *Adv. Funct. Mater.* **2020**, *30*, 1910225.
[6] J. Bang, S. Coskun, K. R. Pyun, D. Doganay, S. Tunca, S. Koylan, D. Kim, H. E. Unalan, S. H. Ko, *Appl. Mater. Today* **2021**, *22*, 100909.
[7] X. Chen, G. Xu, G. Zeng, H. Gu, H. Chen, H. Xu, *Adv. Mater.* **2020**, *32*, 1908478
[8] V. H. Nguyen, D. T. Papanastasiou, J. Resende, L. Bardet, T. Sannicolo, C. Jiménez, D. Muñoz-Rojas, N. D. Nguyen, D. Bellet, *Small* **2022**, *18*, 2106006.
[9] J. J. Patil, W. H. Chae, A. Trebach, K. J. Carter, E. Lee, T. Sannicolo, J. C. Grossman, *Adv. Mater.* **2021**, *33*, 2004356.
[10] C. Celle, C. Mayousse, E. Moreau, H. Basti, A. Carella, J.-P. Simonato, *Nano Res.* **2012**, *5*, 427.
[11] L. Bardet, D. T. Papanastasiou, C. Crivello, M. Akbari, J. Resende, A. Sekkat, C. Sanchez-Velasquez, L. Rapenne, C. Jiménez, D. Muñoz-Rojas, A. Denneulin, D. Bellet, *Nanomaterials* **2021**, *11*, 2785.
[12] J. M. Lee, Y. H. Kim, H. K. Kim, H. J. Kim, C. H. Hong, *Sci. Rep.* **2020**, *10*, 4592.
[13] A. Khan, V. H. Nguyen, D. Muñoz-Rojas, S. Aghazadehchors, C. Jiménez, N. D. Nguyen, D. Bellet, *ACS Appl. Mater. Interfaces* **2018**, *10*, 19208.
[14] Q. Tang, H. Shen, H. Yao, Y. Jiang, C. Zheng, K. Gao, *Ceram. Int.* **2016**, *43*, 1106.
[15] Y. Huang, Y. Tian, C. Hang, Y. Liu, S. Wang, M. Qi, H. Zhang, Q. Peng, *ACS Appl. Nano Mater.* **2019**, *2*, 2456.
[16] S. Aghazadehchors, V. H. Nguyen, D. Munõz-Rojas, C. Jiménez, L. Rapenne, N. D. Nguyen, D. Bellet, *Nanoscale* **2019**, *11*, 19969.
[17] J. A. Resende, A. Sekkat, V. H. Nguyen, T. Chatin, C. Jiménez, M. Burriel, D. Bellet, D. Muñoz-Rojas, *Small* **2021**, *17*, 2007344.
[18] D. T. Papanastasiou, A. Sekkat, V. H. Nguyen, C. Jiménez, D. Muñoz-rojas, F. Bruckert, D. Bellet, *Adv. Mater. Technol.* **2022**, *8*, 2200563.
[19] W. H. Chae, J. J. Patil, J. C. Grossman, *ACS Appl. Mater. Interfaces* **2022**, *14*, 34997.
[20] J. J. Patil, M. L. Reese, E. Lee, J. C. Grossman, *ACS Appl. Mater. Interfaces* **2022**, *14*, 4423.
[21] A. A. Pilarska, L. Klapiszewski, T. Jesionowski, *Powder Technol.* **2017**, *319*, 373.
[22] O. P. Das, S. K. Pandey, *J. Phys.: Conf. Ser.* **2023**, *2426*, 012031.
[23] R. Aouati, H. Djaaboube, A. Bouabelloul, A. Taabouche, Y. Bouachiba, W. Daranfad, A. Oudina, F. Kharfi, *Semiconductors* **2021**, *55*, 583.
[24] M. Kongtungmon, L. Supadee, W. Kundhikanjana, P. Janphuang, R. Supruangnet, S. Tongpeng, W. Jongpinit, D. Munthala, S. Pojprapai, *Mater. Res. Bull.* **2023**, *167*, 112397.
[25] M. Tlili, C. Nefzi, B. Alhalaili, C. Bouzidi, L. Ajili, N. Jebbari, R. Vidu, N. Turki Kamoun, *Nanomaterials* **2021**, *11*, 3076.
[26] Y. Xu, J. D. Mackenzie, *J. Sol-Gel Sci. Technol.* **1997**, *301*, 295.
[27] S.-I. Yamamoto, H. Yoshioka, H. Kosuga, *Trans. Mater. Res. Soc. Jpn.* **2014**, *39*, 339.
[28] W. B. Wang, Y. Yang, A. Yanguas-gil, N. N. Chang, G. S. Girolami, J. R. Abelson, *Appl. Phys. Lett.* **2013**, *102*, 101605.
[29] S. M. George, *Chem. Rev.* **2010**, *110*, 111.
[30] T. Hatanpää, J. Ihanus, J. Kansikas, I. Mutikainen, M. Ritala, M. Leskelä, *Chem. Mater.* **1999**, *11*, 1846.
[31] J.-G. Song, J. Park, J. Yoon, K. Kim, Y. Jang, K. Kim, H. Kim, *J. Alloys Compd.* **2014**, *588*, 716.
[32] B. B. Burton, D. N. Goldstein, S. M. George, *J. Phys. Chem. C* **2009**, *113*, 1939.
[33] W. Kang, B. J. Choi, J. H. Han, *Ceram. Int.* **2020**, *46*, 10115.
[34] B. W. Wang, J. Choi, H. G. Kim, S. D. Hyun, C. Yoo, S. Kim, H. Lee, C. S. Hwang, *J. Mater. Chem. C* **2021**, *9*, 15359.
[35] L. M. Kern, R. Galceran, V. Zatko, M. Galbiati, F. Godel, D. Perconte, F. Bouamrane, E. Gaufrès, A. Loiseau, P. Brus, O. Bezencenet, M. B. Martin, B. Servet, F. Petroff, B. Dlubak, P. Seneor, *Appl. Phys. Lett.* **2019**, *114*, 053107.
[36] R. Huang, A. H. Kitai, *Appl. Phys. Lett.* **1992**, *61*, 1450.
[37] M. Putkoncn, L. S. Johansson, E. Rauhala, L. Niinisto, *J. Mater. Chem.* **1999**, *9*, 2449.
[38] P. Vale, A. Sekkat, T. Gheorghin, S. Sevim, E. Mavromanolaki, A. D. Flouris, S. Pan, D. Mun, J. Puigmart, T. S. Mayor, **2023**, *127*, 9425.
[39] D. Muñoz-Rojas, J. Macmanus-Driscoll, *Mater. Horiz.* **2014**, *1*, 314.
[40] D. Muñoz-Rojas, V. H. Nguyen, C. Masse de la Huerta, S. Aghazadehchors, C. Jiménez, D. Bellet, *C. R. Phys.* **2017**, *18*, 391.
[41] C. A. M. de la Huerta, V. H. Nguyen, A. Sekkat, C. Crivello, C. Jimenez, F. Toldra-Reig, P. B. Veiga, S. Quessada, D. Munõz-Rojas, *Adv. Mater. Technol.* **2020**, *5*, 2000657.
[42] A. Sekkat, V. H. Nguyen, C. Arturo, M. De La, L. Rapenne, D. Bellet, A. Kaminski-cachopo, G. Chichignoud, D. Muñoz-rojas, *Commun. Mater.* **2021**, *2*, 78.
[43] A. Sekkat, M. O. Liedke, V. H. Nguyen, M. Butterling, F. Baiutti, J. De Dios, S. Veru, M. Weber, L. Rapenne, D. Bellet, G. Chichignoud, A. Kaminski-Cachopo, E. Hirschmann, A. Wagner, D. Muñoz-Rojas, *Nat. Commun.* **2022**, *13*, 5322.
[44] A. Schultheiss, A. Sekkat, V. H. Nguyen, A. Carella, A. Benayad, A. Revaux, R. Demadrille, D. Muñoz-Rojas, J. P. Simonato, *Synth. Met.* **2022**, *284*, 116995.
[45] V. S. Nguyen, A. Sekkat, D. Bellet, G. Chichignoud, A. Kaminski-Cachopo, D. Muñoz-Rojas, W. Favre, *J. Mater. Chem. A* **2021**, *9*, 15968.
[46] M. Weber, N. Boysen, O. Graniel, A. Sekkat, C. Dussarrat, P. Wiff, A. Devi, D. Mun, *ACS Mater. AU* **2023**, *24*, 215501.
[47] D. P. Langley, M. Lagrange, G. Giusti, C. Jiménez, Y. Bréchet, N. D. Nguyen, D. Bellet, *Nanoscale* **2014**, *6*, 13535.
[48] G. A. Adebayo, Y. Liang, C. R. Miranda, S. Scandolo, *J. Chem. Phys.* **2009**, *131*, 014506.
[49] J. R. Jasperse, A. Kahan, J. N. Plendl, S. S. Mitra, *Phys. Rev.* **1966**, *146*, 526.
[50] S. S. Kushwah, J. Shanker, *Phys. B: Condens. Matter* **1996**, *225*, 283.
[51] J. Cotton, AZO Materials Homepage, https://www.azom.com/properties.aspx?ArticleID=54, (accessed: February 2001).
[52] C. Mayousse, C. Celle, E. Moreau, J.-F. Mainguet, A. Carella, J.-P. Simonato, *Nanotechnology* **2013**, *24*, 215501.